Revisão

ANODES FOR SOFC: REVIEW OF MATERIAL SELECTION, INTERFACE AND ELECTROCHEMICAL PHENOMENA

Marina Curi[a,*,ID], Eduardo da R. Silva[b,c], José Geraldo de M. Furtado[c], Helen C. Ferraz[b] and Argimiro R. Secchi[b]

[a]Escola de Química e Alimentos, Universidade Federal do Rio Grande, 96203-000 Rio Grande – RS, Brasil
[b]Centro de Tecnologia, Universidade Federal do Rio de Janeiro, 21941-972 Rio de Janeiro – RJ, Brasil
[c]Centro de Pesquisa em Energia Elétrica, 21941-911 Rio de Janeiro – RJ, Brasil

This paper presents a comprehensive interface and electrochemical phenomena review of different anodes for SOFC. In this way, it was possible to select some mixed electronic and ionic conductor materials alternatives to the conventional anode, Ni-YSZ conductor. New materials must present a satisfactory electronic and ionic conductivity at intermediate temperatures, be able to operate under different types of hydrocarbon fuels without deactivation, present stability under redox cycles and thermal expansion compatible with the other materials. Among all new materials, $Sr_{0.86}Y_{0.08}TiO_3$, a Y-doped strontium titanate (YST), presented the highest measured conductivity, of 82 S cm^{-1} at 800 °C. In addition, this material showed excellent stability time and coefficient of thermal expansion compatible with materials used as cathode, strontium-doped lanthanum manganite and electrolyte, yttria stabilized zirconia. $SrTiO_3$ (ST) compounds synthesized by solid-state reaction method, calcined, and sintered to obtain undoped (ST), 4% (YST04) and 8% (YST08) of Y-dopant and as a heterojunction with yttria-stabilized zirconia (YST08/YSZ). It was observed that calcination under Ar/5%H$_2$ atmosphere has increased the dopant maximum concentration in the $SrTiO_3$ cubic crystal structure when compared to inert atmosphere. When the Y solubility limit was exceeded, a pyrochlore phase $Y_2Ti_2O_7$ was formed on the intergranular region due to the deficiency of oxygen vacancies, especially in the presence of inert atmosphere.

Keywords: anode; interfacial phenomena; MIEC; SOFC.

INTRODUCTION

One of the main characteristics that affect solid oxide fuel cell (SOFC) performance is the structure of its electrodes (anode and cathode). Such characteristics are determined by the type of the structure utilized and its manufacturing process. Moreover, the electrochemical reactions that occur on the anode surface and on the interface of anode/electrolyte are different from other heterogeneous reactions.[1] Thus, it is necessary to study how the anode behaves on microscopic and nanoscopic scales.

For more than forty years, Ni-YSZ *cermet* composites have been the main anode applied to SOFCs due to their excellent catalytic activity with hydrogen fuel, high electronic conductivity,[2] reasonable

ionic conductivity at high temperature, stability under the conditions of SOFC operations and relatively low manufacturing cost. This material has shown a satisfactory performance when compared to many other applied *cermets* such as Ru/ZrO2, Mg-YSZ, and pure Ni. In this *cermet* conventional anode, the chemical reaction occurs on a three-phase boundary (3PB) defined as an interface composed by an oxygen-ion conductor phase YSZ (electrolyte), an electronic conductor phase (Ni metal) and a fuel gas phase. If the oxygen-ions or the fuel gas molecules do not reach the reaction site, or the electrons cannot be removed from the site, then the 3PB is not able to contribute to the good performance of the SOFC (see Figure 1).

However, there are many limitations to the use of Ni-YSZ as an anodic material, mainly including a Ni agglomeration in a long-term
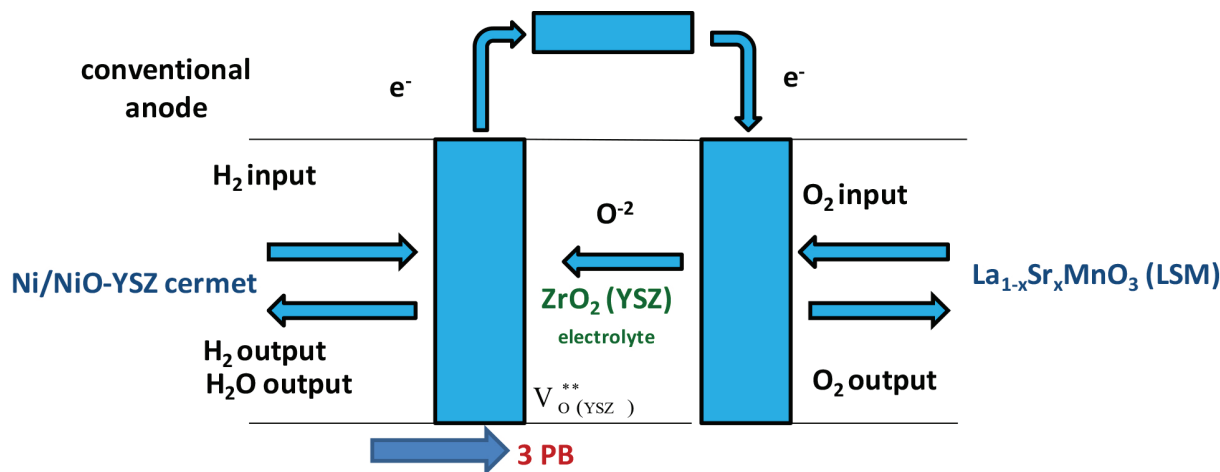

Figure 1. Simplified scheme of a SOFC applying conventional anode

*e-mail: marinaoliveiracuri@gmail.com

operation and the formation of carbon deposits with the breaking of the C-C bond with the use of hydrocarbons. Ni is an excellent catalyst; therefore, carbon is deposited on the Ni surface, diffusing the Ni particle structure, and leading to the formation of carbon filaments,[3] bringing the impossibility to operate using hydrocarbon fuels.

In this sense, in mixed ionic and electronic conductors (MIEC), charge carriers are combined in one single phase. In this type of material, ionic conductivity can be one order of magnitude higher than in conventional materials as YSZ, which allows decreasing the operation temperature, improving the SOFC performance and durability, as well as, making it possible to reduce the manufacturing costs of this fuel cell. Moreover, these materials can extend the active electrochemical regions for whole electrode surface. MIEC performs both as catalyst and as electrons and ions carrier. The electrochemical reactions are not restricted to the conductor interface but can occur along the entire surface.[4]

Comparing Figure 1 with Figure 2, it can be noted that the oxygen vacancy region, using MIEC as an anode, is not only restricted to the anode/electrolyte interfacial region $V_{O(YSZ)}^{**}$, but it is also present along the anode thickness of (l_a) $V_{O(MIEC)}^{**}$.

Figures 3 and 4 present micrographs of a potential material composed by 8% Y-doped SrTiO$_3$. It is possible to notice a well-defined grain boundary with an efficient interface formation between YSZ and YST08 grains, showing that both are compatible with no physical segregation. Another important characteristic shown in the structure is the possibility of assembling samples with porosity among 20 – 40 %. In 8% Y-doped SrTiO$_3$, porosity of 36.7 ± 7.2 % was found using 10% w/w of graphite before the sintering process. It is possible to observe that there is wide pore network, this feature is important to maintain the fuel gas diffusivity and the product exhaustion.

SOFC anodes

The YSZ grains constitute a support which acts as an inhibitor to the sintering of Ni powders during the SOFC operation, since the Ni thermal expansion coefficient (TEC), 16.9×10^{-6} K^{-1}, is higher than that of YSZ (11×10^{-6} K^{-1}). Therefore, the use of YSZ makes the TEC of the Ni/YSZ composite close to the other components of the SOFC. Additionally, due to the high electronic conductivity of Ni, the ionic conductivity of the material is improved, since the proportion in volume percentage of Ni and YSZ ranges from 35:65 to 55:45, providing a conductivity of the material ranging from 0.1 to 10^3 S cm^{-1}.[5]

The poisoning of the Ni/YSZ anode by impurities containing sulfur in the H$_2$ current has been studied using electrochemical impedance spectroscopy (EIS) and direct current (DC) polarization method. There are models that describe the loss of electrode performance due to the presence of H$_2$S, however, according to Matsuaki and Yasuda,[6] the exact mechanism responsible for the loss of performance
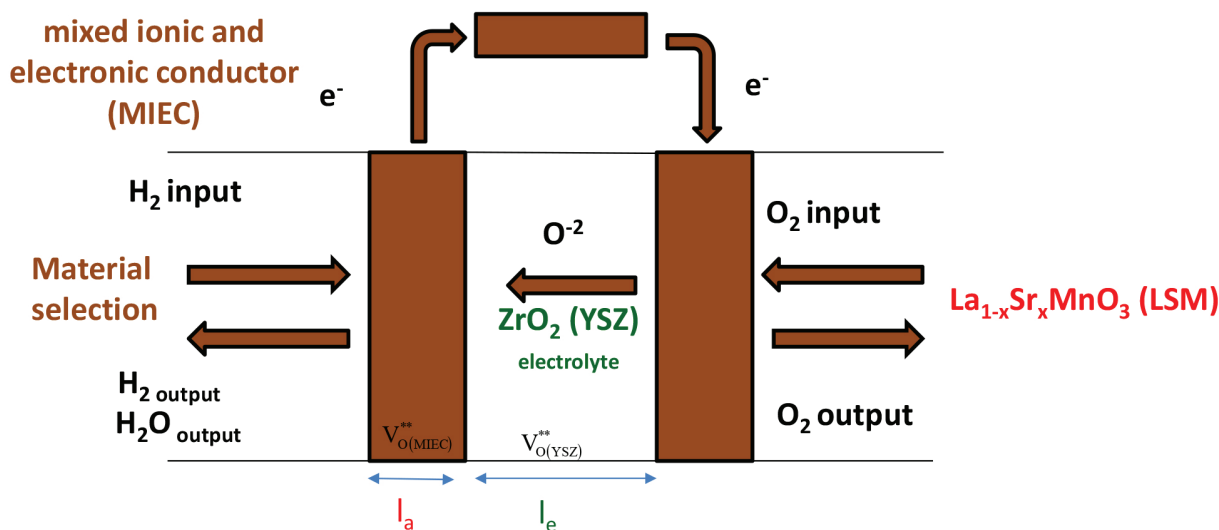

Figure 2. *Simplified scheme of a SOFC applying MIEC anode*
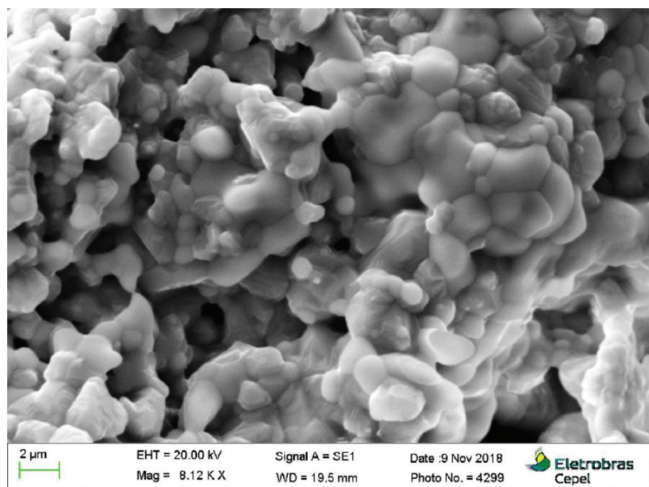
**Figure 3.** *YSZ/YST08 heterojunction using graphite – porosity 27.01%*
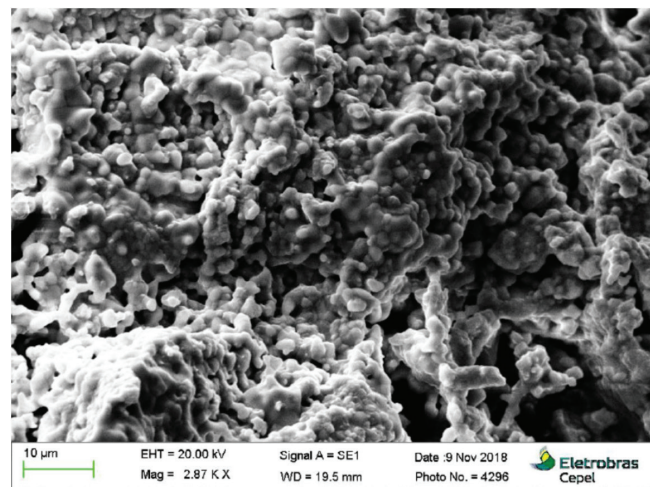
Figure 4. *YSZ/YST08 heterojunction using graphite – porosity 38.82%*

is not clearly defined yet due to the lack of experimental data in these specific conditions. The polarization resistance and electrode overpotential increased when the H₂S concentration exceeded 0.05, 0.5 and 2 ppm at 1023, 1173 and 1273 K, respectively. The time required for the sulfide to influence saturation was approximately 3 hours and 20 minutes, 2 hours and 30 minutes, and 1 hour at 1023, 1173 and 1273 K, respectively. Although there are many benefits in reducing the operating temperature, it must be considered that at low temperatures the sulfides can be strongly adsorbed on the surface of the anode electrode of the SOFC and degrade the resistance against impurities (sulfides) reducing the conductivity due to microstructural degradation. This was later confirmed by Lussier *et al.*[7] who showed a mechanism that reveals the degeneration of Ni/YSZ and Ni/GDC anodes exposed to H₂S, thus compromising the electrical conductivity of the anode and, consequently, the SOFC performance.

According to Flores and Rodríguez[8] and Tarôco *et al.*,[5] in general, the anode must meet the following requirements:

- High electronic conductivity (~ 100 S cm^{-1});
- Chemical stability at low oxygen partial pressures (10^{-20} bar) and with other fuel cells (FC) components (electrolyte and interconnector);
- High catalytic activity for oxidation reaction of the selected fuel gas;
- Coefficient of thermal expansion similar to other components;
- Ability to avoid carbon deposition;
- Optimization of the electric transport microstructure (ionic + electronic);
- Stability in reducing environment;
- It must be thin enough to transport mass and minimize ohmic losses, but also have a certain thickness to distribute the electric current;
- Adequate porosity (20-40%) for fuel supply and removal of the product from the reaction.
- The anode, besides providing the electrochemical reaction of oxidation of the fuel, must also transfer the electrons. The oxygen anions migrate, through the electrolyte, from the cathode to the anode, due to the potential difference, where they are consumed by the oxidation of the fuel according to the following reactions:[9]

$$H_2 + O^{-2} \rightarrow 2e \tag{1}$$
$$CO + O^{-2} \rightarrow 2e \tag{2}$$
$$C_nH_{(2n+2)} + (3n + 1)O^{-2} \rightarrow nCO_2 + (n + 1)H_2O + (6n + 2)e \tag{3}$$
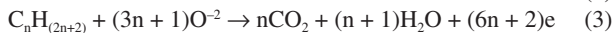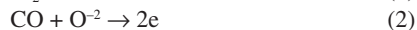
As showed in Equations 1 and 2, two electrons are transferred for each mole of water and CO₂ formed, respectively. The molar flow rate of water (R_{H_2O}) and CO₂ (R_{CO_2}) formation can be determined by Faraday's Law (Equations 4 and 5). Details on the development of these equations can be found at Curi.[10]

$$R_{H_2O} = \frac{i}{2F} \tag{4}$$

$$R_{CO_2} = \frac{i}{2F} \tag{5}$$

where i is the current drained by a charge coupled to the FC unit and F is the Faraday constant.

Regarding those problems, new materials should be researched and applied to replace Ni-YSZ-based anodes, focusing mainly on compounds that are flexible to the type of fuel used, and those more resistant to sulfur impurities, and also suitable for operation in low temperatures and long-term operation. The different SOFC anodes found in the literature are presented.

Perovskite anodes

The crystalline structure of a perovskite has the composition ABX₃, where A and B are cations with different oxidation numbers and X is an anion.[11] B cation occupies the cell unit center, while A cation and X anion occupy the vertices and edges of the unit cell, respectively.[12,13] A typical perovskite is exemplified with the structure of SrTiO₃ in Figure 5. Due to steric impediments from combinations of different ions, with different ionic radius, perovskite structures can present different degrees of distortions that even lead to different crystalline systems.
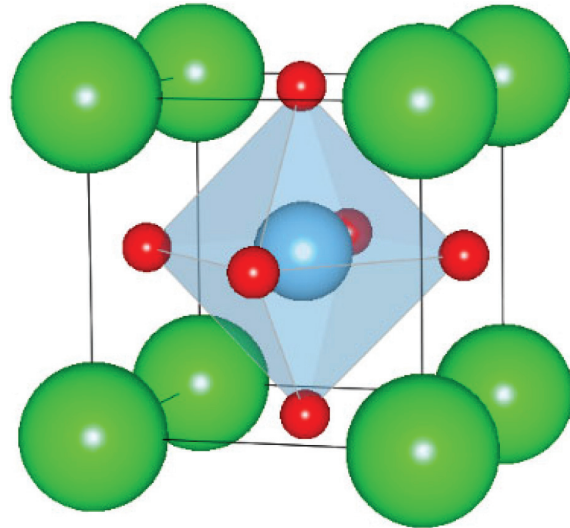
Figure 5. *Crystalline structure of strontium titanate (SrTiO₃), Sr atoms are represented by green spheres, O atoms in red and Ti in blue. Adapted from ref. 14*

Vashook *et al.*[15] synthesized a series of perovskite-type compounds La$_{1-a}$Ca$_a$Cr$_{0.2}$Ti$_{0.8}$O$_{3-\delta}$ by the solid-state reaction technique (calcination temperature of 1350 °C). The increase in the concentration of Ca decreases the thermal stability of the oxides related to the dissociation of oxygen. The maximum conductivity observed was 50 S cm^{-1} for a composition of a = 0.95 of dopant. This Ca composition corresponds to a Cr^{3+}/Cr^{4+} = 1 ratio, oxygen stoichiometry (3-δ) = 3 and the oxidation states of La, Ca and Ti ions of 3+, 2+ and 4+, respectively. In reducing atmosphere, the maximum conductivity is observed with a concentration of a = 0.6 of dopant, corresponding to the ratio of Ti^{3+}/Ti^{4+} = 1, oxygen stoichiometry (3-δ) = 2.92 and the oxidation states of La, Ca and Ti of 3+, 2+ and 3+, respectively. The change in conductivity of La$_{1-a}$Ca$_a$Cr$_{0.2}$Ti$_{0.8}$O$_{3-\delta}$ from n-type to p-type occurs with an increase in Ca content from a = 0.7 to a = 0.9. In addition, a change in the type of conductivity with a = 0.8 was observed in extremely reducing atmospheres p$_{O2}$ < 10^{-10}, where the conductivity is n-type (slope of the log(σ) versus log(p$_{O2}$) is negative), while in oxidizing atmospheres La$_{0.2}$Ca$_{0.8}$Cr$_{0.2}$Ti$_{0.8}$O$_{3-\delta}$ becomes a p-type semiconductor.

In Vashook *et al.*[16] work, two series of perovskite La$_{(1-x)}$Ca$_x$TiO$_3$ (x = 0.2 − 1) and La$_{2(1-x)/3}$Ca$_x$TiO$_3$ (x = 0.2 − 1) compounds were synthesized by the solid-state reaction technique (calcination temperature of 1350 °C). Perovskite La$_{0.4}$Ca$_{0.4}$TiO$_3$ revealed a tetragonal structure between 470 K and 1070 K, and cubic at 1170 K. The structure of the perovskite La$_{2(1-x)/3}$Ca$_x$TiO$_3$ is stabilized with small amounts of Ca. Point defects are considered for La$_{(1-x)}$Ca$_x$TiO$_{3-\delta}$ and La$_{2(1-x)/3}$Ca$_x$TiO$_3$. The n-type conduction can be explained by the creation of defects, associated with the reduction of Ti^{4+} to Ti^{3+} by the removal of oxygen (Equation 6):

$$2Ti_{Ti}^x + O_O^x \leftrightarrow 2Ti_{Ti}^{'} + V_{\ddot{O}} + 0.5O_2 \tag{6}$$

Huang *et al.* (2006a)[17] showed that each oxygen vacancy reduces 2 moles of Mo^{6+} to Mo^{5+}, providing good electronic conductivity to $Sr_2MnMoO_{6-\delta}$ and $Sr_2MgMoO_{6-\delta}$ anodes. In the same work, it was found that the electronic conductivity decreases with the increase in the partial pressure of O_2, but the conductivity of the $Sr_2MnMoO_{6-\delta}$ was more sensitive to pressure variation.

In Lepe *et al.*[18] work, oxides with the general formula $Ln_{2/3-x}TiO_{3-3x/2}$ (Ln = La, Pr and Nd; $0.07 \leq x < 0.13$) were prepared by a new synthesis route, adding $Ln_{2/3-x}Li_{3x}TiO_3$ precursors, prepared by two methods: solid-state reaction and sol-gel (modification of the Pechini process),[19] followed by dehydration and calcination steps. Results from EIS showed that the resistance in the grain boundaries three times greater than that of the bulk for the lanthanum and praseodymium titanates. Comparing the two titanates, it was concluded that the resistance in the grain boundary region with La is smaller than that with Pr. This result can be attributed to small structural differences since the diffractogram of the compound with Pr shows peaks attributed to the tetragonal phase. The type of imperfections depends on the way the crystal was formed. Defects modify the electrical behavior of the material. Results presented proved that the conductivity in the bulk of the compound with La is greater than that with Pr.

Pudmich *et al.*[20] investigated materials with perovskite-type structures based on lanthanum chromates and strontium titanates as possible materials for SOFC anodes. Table 1 shows the studied materials. It was found that the higher the concentration of Ti, the greater the electronic conductivity of the material while the increase in the concentration of Cr reduces the electronic conductivity of the same compound. In samples rich in Cr, the electronic conductivity in air was higher than in the presence of H_2. Thus, as a p-type conductor (excess of electron holes), conductivity is decreased in reducing atmospheres due to the reduction in electron holes in combination with increased O_2 vacancy concentration. In the case of Ti-rich samples, conduction is n-type (excess of electrons) and charge carriers (electrons) are formed during the reaction. EIS measurements and analysis showed a certain activity of the $La_{0.7}Sr_{0.3}Cr_{0.8}Ti_{0.2}O_3$ electrode on hydrogen oxidation, but the performance remained low when compared to the Ni-YSZ composite.

Chen and Liu[21] evaluated the conductivity of $La_{0.9}Sr_{0.1}Ga_{0.8}M_{0.2}O_3$ (LSGM) with M = Co, Mn, Cr, Fe or V. Among the transition metals studied, the samples doped with Mn and Co showed conductivity larger than the other samples. $La_{0.9}Sr_{0.1}Ga_{0.8}Mn_{0.2}O_3$ presented the highest conductivity in the bulk. $La_{0.9}Sr_{0.1}Ga_{0.8}Co_{0.2}O_3$ disintegrated under H_2-reducing conditions and cannot therefore be used with anodic material. Among the different dopants for $LaGaO_3$, Co resulted in the highest conductivity in air, while Mn provided the highest conductivity in a reducing atmosphere. Electrochemical measurements showed that $La_{0.9}Sr_{0.1}Ga_{0.8}Mn_{0.2}O_3$ is a MIEC material with significant ionic conductivity, ionic and electronic resistance at 780 °C of 2.47 Ω and 9.47 Ω, respectively, while $La_{0.9}Sr_{0.1}Ga_{0.8}Co_{0.2}O_3$

presented high electronic conductivity (ion transfer number less than 1), ionic and electronic resistance at 780 °C of 33.56 Ω and 2.43 Ω, respectively.

In Chen and Liu[21] work, oxides of transition metals were doped with $LaGaO_3$ in order to increase electronic conductivity while maintaining ionic conductivity, LSGM can be used as MIEC for SOFC and its use has two advantages: first, they are chemically and physically compatible with LSGM electrolytes, minimizing interfacial reactions due to diffusion or chemical reaction; second, their coefficients of thermal expansion are similar to that of the electrolyte, minimizing stress at the interface during the thermal cycle and, thus, improving the adhesion between the electrode and the electrolyte. However, measures of thermal expansion coefficients were not presented in that work.

$La_xSr_{1-x}CrO_3$ (LSC) has good stability in an anodic environment, however, $La_xSr_{1-x}MnO_3$ (LSM) has high electronic conductivity but is not stable in reducing atmospheres. For this reason, metal oxides with $La_{0.75}Sr_{0.25}Cr_{1-x}Mn_xO_3$ (LSCM) composition (x = 0.4, 0.5, 0.6) were synthesized and examined as anode material for SOFC.[22] $La_{0.75}Sr_{0.25}Cr_{0.6}Mn_{0.4}O_3$, $La_{0.75}Sr_{0.25}Cr_{0.5}Mn_{0.5}O_3$ and $La_{0.75}Sr_{0.25}Cr_{0.4}Mn_{0.6}O_3$ powders were synthesized by the glycine combustion. It was found that the conductivity of the anode increases with the partial pressure of oxygen and decreases with the Cr content. The densified samples show no differences in morphology. However, the crystalline structure changed from hexagonal, in air, to orthorhombic, in a reducing environment. In that same work, the LSCM tolerance to H_2S was measured, introducing 10% H_2S into the hydrogen stream and the results showed that under open-circuit conditions the reaction products (MnS and MnOS) are conductive, which can reduce the resistance and improve the supply of electric current. This phenomenon can be explained because SOFC obtained a small increase in its performance after being fed with fuel contaminated with sulfur. However, under potentiostatic conditions (control of the voltage difference between the working electrode and the reference electrode with current injection), the intermediate species and the products formed can accelerate anode poisoning, especially in the 3PB.

The physical properties and the level of mixed conduction presented by the compounds $Sr_{0.97}Ti_{0.6}Fe_{0.4}O_{3-\delta}$ (STFO) and $La_{0.4}Sr_{0.5}Ti_{0.6}Fe_{0.4}O_{3-\delta}$ (LSTFO) were studied by Fagg *et al.*[23] The powders were prepared by the solid-state reaction from TiO_2, Fe_2O_3, La_2O_3 and $SrCO_3$. STFO was sintered at 1400 °C and LSTFO at 1600 °C. The use of the highest temperature for LSTFO is necessary to achieve phase purity and good densification. Deficiency at the A site (La and Sr in LSTFO, and Sr in STFO) was introduced in both compositions, with a unit ratio of A/(Ti + Fe), in order to improve the stability of these materials. The lowest total conductivity for LSTFO was observed, which can be attributed to the low concentration of electron holes under oxidation conditions. The main factor that affects the level of ionic conduction is the high activation energy of

Table 1. Name, chemical composition, and crystallographic properties of the powders after sintering 1400 ºC. Adapted from ref. 20

Acronym	Composition	Crystal system	Lattice constant(Å)	Secondary phase
LCCT-7382	$La_{0.7}Ca_{0.3}Cr_{0.8}Ti_{0.2}O_3$	Orthorhombic	a=5.4663 b=5.4755 c=7.7309	
LCCT-7355	$La_{0.7}Ca_{0.3}Cr_{0.5}Ti_{0.5}O_3$	Orthorhombic	a=5.4736 b=5.4837 c=7.7459	
LCCT-7328	$La_{0.7}Ca_{0.3}Cr_{0.2}Ti_{0.8}O_3$	Not determined		$La_4Ca_2Ti_5O_{18}$
LCT-73X	$La_{0.7}Ca_{0.3}TiO_3$	Not determined		$La_4CaTi_5O_{17}$
LCCF-7382	$La_{0.7}Ca_{0.3}Cr_{0.8}Fe_{0.2}O_3$	Orthorhombic	a=5.4587 b=5.4776 c=7.8287	
LCCV-7382	$La_{0.7}Ca_{0.3}Cr_{0.8}V_{0.2}O_3$	Orthorhombic	a=5.4693 b=5.4817 c=7.7167	$Ca_2La_{0.67}(VO_4)_2$
LSCT-7382	$La_{0.7}Sr_{0.3}Cr_{0.8}Ti_{0.2}O_3$	Hexagonal	a=5.5047 c=13.3504	

LSTFO, which may be due to the significant formation of vacancy mobilities, in addition, the increase in temperature should increase the concentration of vacancies present. It should also be considered that LSTFO exhibits an orthorhombic structure while STFO exhibits cubic structure. These two structures do not exhibit the same enthalpy for ion migration and vacancy formation. However, the polymorphism change is not related to the high activation energy. Examples against this hypothesis are that compounds such as $La_{0.9}Sr_{0.1}Ga_{0.8}Mg_{0.2}O_{3-\delta}$ with orthorhombic structure, still exhibit high levels of ionic conductivity with activation energy around $100\ kJ\ mol^{-1}$. In that work, the ionic conductivity was separated from the total conductivity by using the Faradaic efficiency, based on EIS measurement data, presented in Kharton *et al.*[24] The number of ions transfer ranged from 0.005 to 0.08 to $Sr_{0.97}Ti_{0.6}Fe_{0.4}O_{3-\delta}$, decreasing as the temperature decreases. The conductivity of the electron holes of the oxide was small, but exceeded the ionic conductivity, showing that the behavior of the p-type semiconductor was more pronounced. The activation energy for the electronic conductivity was $35\ kJ\ mol^{-1}$ between 470 and 890 K (calculated by the Arrhenius model), being reduced to higher temperatures. Thermogravimetric analysis (TGA) in different atmospheres showed that at temperatures above 770 K the $Sr_{0.97}Ti_{0.6}Fe_{0.4}O_{3-\delta}$ perovskite phase is stable concerning the reaction with CO_2. However, the exposure of STFO powders to lower temperatures can result in the decomposition of its surface associated with the formation of $SrCO_3$.

Ruiz-Morales *et al.*[25] studied the substitution of Ti in $La_4Sr_8Ti_{12-x}M_xO_{38-\delta}$ with M = Mn, Ga or Sc controlling oxygen stoichiometry. The best composition for the lowest polarization resistance observed for the oxide was M = Ga and x = 0.5 ($La_4Sr_8Ti_{11.5}Ga_{0.5}Mn_{0.5}O_{37.5}$) (LSTMG) both in reducing conditions with H_2 fuel (2.3% v/v H_2O) as with CH_4 (2.3% v/v H_2O), presenting a lower polarization resistance of 0.20 and 0.57 $\Omega\ cm^2$, respectively, which were less than for x = 0 (2.97 and 8.93 $\Omega\ cm^2$, respectively), M = Sc and x = 0.6 (0.5 and 1.20 $\Omega\ cm^2$, respectively) and M = Mn and x = 1 (0.43 and 1.14 $\Omega\ cm^2$, respectively). Mn and Ga have lower coordination numbers (fewer neighboring atoms), especially Mn^{3+}, and thus facilitate the migration of the oxygen ion. Thus, with the addition of Mn and Ga, MIEC is promoted by accelerating the electrocatalytic processes at the interfaces.

In the study by Vernoux *et al.*,[26] $La_{0.8}Sr_{0.2}Cr_{0.97}V_{0.03}O_3$ anode (LSCV) in the conversion of methane exhibited low activity at 800 and 850 °C, but no carbon deposition was detected after 30 h of operation. EIS measurements of the LSCV-YSZ composite showed that the high-frequency semicircle (HF) is probably related to the electrode/electrolyte microstructure interface, while the medium frequency semicircle (MF) may be associated with electrochemical reaction in 3PB.

In the article by Vernoux *et al.*,[27] LSC, LCR and LSCM powders with a nominal composition of $La_{0.8}Sr_{0.2}CrO_{3-\delta}$, $LaCr_{0.95}Ru_{0.05}O_{3-\delta}$ and $La_{0.8}Sr_{0.2}Cr_{0.8}Mn_{0.2}O_{3-\delta}$, respectively, were synthesized by spray pyrolysis (ultrasonic atomization technique) and the films were prepared by spray printing (deposition and printing from atomized powders). Results of catalytic activity prove that the insertion of Ru in the structure accelerates the methane reform. The thermal behavior of $La_{0.8}Sr_{0.2}CrO_{3-\delta}$ (LSC) was assessed using dilatometry. At 500 °C, a contraction was observed, probably due to the decomposition of $LaNO_3$. LSC X-ray diffractometry (XRD) studies have shown the presence of $MCrO_4$ (M is La or Sr), which is a product of the decomposition of chromium and lanthanum nitrates in the air. In the XRD of LSC powders prepared by spray pyrolysis (SP), the investigated phase of LSC was visible after SP at 800 °C for 8 s. The presence of a secondary phase can be attributed to the presence of the monoclinic structure SrO_4, or the solid solution, such as lanthanum

or strontium chromates. Other results show that the secondary phase disappeared after 1100 °C for 4 hours.

TGA curves showed in mass loss between 750 °C and 780 °C, in that same temperature range, there was a drop in the dilatometric curve. In this way, it can be said that the chromates of La and Sr were completely transformed into LSC between 750-780 °C to 1230 °C. Chromatographic analyzes showed two peaks of CO and CO_2 for the Ni-YSZ anode and only one peak of O_2 for LSCM, this means that the carbon formed by the coke reaction is present on the Ni-YSZ surface. Results from EIS showed that Mn insertion improves the electrochemical activity of perovskites. LCR was not investigated via EIS due to its low electronic conductivity (no Sr content).[27]

Sfeir[28] analyzed the stability of $LaCrO_3$ when doped with Mg, Ca, Sr, Mn, Fe, Co and Ni against various atmospheres (air, humidified hydrogen, CO and CO_2). Experimental and thermodynamic data showed at the A-site, the substitution of Sr is more stable than that of Ca in reducing atmospheres since the solubility limit of Ca is low under partial pressure of O_2 at 10^{-9} atm at 1600 °C. CO and CO_2 did not affect the stability of these perovskites, once there is no carbon formation and secondary phases were observed. H_2O and H_2 cause corrosion in these perovskites because the volatility of Ca, Sr and Cr is pronounced due to the formation of hydroxyls. The secondary phases formed during the decomposition can react quickly with YSZ at 800 °C, although the substituting compounds of the B-site (Mg, Mn, Fe, Co and Ni) have shown to be more thermodynamically unstable.

Ceramics with perovskite-type structures, such as $SrTiO_3$, have a great possibility of improving and/or altering their physical and chemical properties and characteristics through doping processes aiming application as SOFC anodes. Doping cations introduce mixed valences and oxygen vacancies into the unit cell. However, when doping those structures, the stability of the material is altered, since the insertion of impurity ions causes distortions in the structural geometry of the crystal lattice, as they present ionic radii that differ from the original configuration.[29-31] In the A–site, in order to accommodate an ion with an ionic radius greater than the ionic radius of Sr the TiO_6 octahedron elongates slightly. Because of this, the Ti ion is no longer the center of symmetry of the unit cell.[32] When ions with an ionic radius smaller than the ionic radius of Sr or with an ionic radius smaller than that of Ti are introduced at sites A and B, respectively, the tolerance factor (T) becomes smaller than 1. In this case, the ion located at site A no longer contacts the 12 oxygen ions. Then the structure adjusts by performing rotations in the TiO_6 octahedron, to maintain the regularity of the structure and the correct sharing of spaces between the ions, so that the ions coming from the TiO_6 octahedron approach the smaller ion now located at A-site.[33] This rotation in the structure has as the main consequence (besides the loss of symmetry); the change in the angle of the Ti-O-Ti connection from 180° to approximately 165°. This effect also leads to a decrease in the coordination number of the A-site cation from 12 to a value between 8 and 10. Both effects alter the electrical characteristics of the material, as they will change the interatomic distances, leading to changes in the band diagrams and in the strength of the Ti-O-Ti bond.[29]

Perovskite structures such as $SrTiO_3$ in their stoichiometric form (Sr/Ti = 1, O/Sr = 3) have a bandgap of 3.2 eV at 0 K. They are considered a proper material for applications as an insulator.[34,35] By convention, it is considered that all compounds with a bandgap above 2 eV are insulator, and less than that, semiconductor (remembering that in metallic materials there is no bandgap due to an overlap of the conduction and valence bands).[36] When there is no compensatory distortion in the TiO_6 octahedron, the highest occupied molecular orbital (HOMO) that corresponds to the valence band is predominantly atomic (2s and 2p oxygen orbitals). The conduction band, which corresponds to the lowest unoccupied molecular orbital

(LUMO), is predominantly cationic and it comes from the unoccupied energy states of the Ti-d orbital. Such difference between the states of HOMO and LUMO is what characterizes $SrTiO_3$ as a robust insulator (dielectric).

There are many studies on the doping process at B-site, mainly with the substitution by cations of $Fe^{3+/2+}$ and Al^{3+}. Synthesis of B-sites doped $SrTiO_3$ structures is widely applied in order to change the ionic and electronic transport properties of the material. Normally, cations with a valence greater than or equal to 3+ are used and the structure is compensated by the formation of oxygen vacancies. Kharton et al.[37] used iron ions to perform the doping process at site B, and a decrease in the size of the crystalline cell due to the steric compensations was noted. The authors observed that the structure had an increase in ionic and electronic conductivities, showing that such doping is advantageous. The activation energy for ionic conductivity was independent of the dopant concentration and it has varied from 97 to 104 kJ mol^{-1}. The TEC is feasible with that relative to the YSZ (1.05×10^{-5} K^{-1}):[38] in a temperature range between 300 and 720 K, they have found 1.2×10^{-5} K^{-1} to the minor concentration of dopant and 2.1×10^{-5} K^{-1} to 8% Fe. Kharton et al.[37] were based on studies by Steinsvik et al.[39] They have doped the titanate structure with iron concentrations that varied from 0 to 8% and concluded that the structures compensate for the charge imbalance with the formation of oxygen vacancies. When the doping concentration was greater than 6%, a crystalline cell was formed, characterized as a superstructure with a lattice constant twice than the one from the simple perovskite. This phenomenon was associated due to structural reorganization from the accumulation of oxygen vacancies. The authors have also concluded that the high level of mixed ionic/electronic conductivity makes this material able to use as an electrode of SOFC.

Doping processes with Fe cations are the most representative model for doping with acceptors in $SrTiO_3$ electroceramics with wide bandgap. The mixture of valence Fe^{3+} and Fe^{2+} creates a series of imbalances with the charges. This will be compensated by the creation of oxygen vacancies whose concentration varies according to the partial pressure regime of oxygen. Kubacki et al.[40] studied the influence of Fe insertion in the $SrTiO_3$ band structure and concluded that Fe^{+3} and Fe^{+2} affect energy bands differently. The first results in a peak-shaped energy state just above the top of the valence band, while the second results in a wider-shaped state in the prohibited band just below 0.5 eV. No state in the Fermi energy region has been created, although there is a hybridization between the Ti and Fe and Ti orbitals and oxygen vacancies, these generate new electronic states proportional to the Fe concentration. Baker et al.,[41] studying the influence of Fe ions on the position of Fermi energy, concluded that when the Fe atom is at the Ti (Fe_{Ti}) site, it assumes valences that can vary from 1+ to 2- in its new energetic state in the middle of the bandgap, this is in the position of 1.7 eV above the top of the valence band. Li et al.,[42] aiming at the application of $SrTiO_3$ structures in the anode compartment of a SOFC, inserted iron cations at B-site and concluded that the conductivity increased proportionally with the increase in the concentration of impurity and the increase in temperature up to the maximum by around 800 °C then started to decrease. Such conductivity profile in relation to the increase in temperature indicates a predominance of concentration of holes as mainly a source of generation of electrical conductivity.

The study of the influence of Al^{3+} ions has also been shown to be representative in the synthesis of extrinsic p-type semiconductors of $SrTiO_3$ electroceramics. Morin and Oliver[43] studied the formation of energy levels in the forbidden band with the introduction of aluminum atoms. An energy level of holes (also called an electron trap) was identified below the beginning of the conduction band with 0.3 eV. This band showed a higher density of holes at 0.09 eV below conduction.

Zhao et al.[44] found that the incorporation of Al^{3+} reduces the possibility of recombination between Ti^{3+} and Ti^{4+}, however, in contrast, it decreases Fermi energy by approximately 0.5 eV. The influence of aluminum ions in the structure will depend on their respective locations in relation to oxygen vacancies: if the oxygen vacancy is surrounded by less than two Al^{3+} ions, adjacent Ti^{4+} ions are formed, generating a complex $\{Ti^{4+}/V_O\}$. However, due to Fermi's low energy, these states are not permanently occupied by electrons, and can, therefore, promote electron-hole recombination. Bowes et al.,[45] when publishing a collection of physicochemical and band information of various types of impurities in $SrTiO_3$ structures, showed that when inserting Al^{3+} ions into the Ti site, Fermi energy is located in values between 0.01 and 0.15 eV, depending on the compensation mechanism of the structure to recover the load balance.

There are also promising studies on doping with niobium (Nb^{5+}): Smith et al.[46] synthesized $SrTiO_3$ structures doped with Ta^{5+} at concentrations of 1%, 5% and 10%. The authors concluded that the lattice constant increases proportionally with the increase in the concentration of dopant and this happens due to the fact that, instead of the replacement of Ti^{4+} by Ta^{5+}, there is an electronic compensation that occurs by converting Ti^{4+} to Ti^{3+} and the latter presents greater ionic radius. Such a mechanism is favored by the presence of reducing agents in the atmosphere, leading to the simultaneous formation of oxygen vacancies. The authors also studied the compatibility between the synthesized structures and YSZ and observed that there was no additional phase or chemical and/or physical segregation on the interface.

Zhang et al.,[47] in their results, showed that with the insertion of Nb, the Fermi level moves considerably towards the conduction band, due to the accumulation of electrons; that is generated with the incorporation of defects. The valence band will consist of the states O 2p and the conduction band will be formed by the states Ti 3d and Ti 4d. Blennow et al.[48] studied the transport of defects and electrons in $SrTiO_3$ structures doped with Nb, the authors showed that the concentration of Nb directly affects the density of states close to the Fermi energy, changing it to energies with values closer to the conduction band. The compensation mechanisms consisted in the presence of electronic exchange (Ti^{4+} atoms are reduced to Ti^{3+}), with no vacancy formation. The Nb atoms remain with fixed oxidation and the partial pressure of oxygen has no direct influence on conductivity. The authors also found evidence that the presence of niobium intensifies the overlapping of the atomic Ti orbitals, intensifying the electrical conductivity of the structure. Ozdogan et al.[49] showed that, in addition to the energy levels mentioned above, niobium influences the conduction band more through the overlapping of the Ti 3d and Nb 4d energy states than in the valence band. Blennow et al.[48] applied structures of $SrTiO_3$ doped with Nb at the B-site in SOFC anodes, and they have not obtained catalytic activity for the redox reactions. Smith et al.[46] studied the effect of doping with tantalum on the operation as an anode of a SOFC and they obtained good chemical compatibility with the electrolyte of YSZ during the redox cycles.

Regarding the doping of A-site, there are many studies about the insertion of lanthanum as an electron donor. Biswas et al.[50] studying this structure with 10% of dopant have found a Fermi energy of 0.2 eV from the base of the conduction band. The authors have stated that negative charge carriers were inserted in the structure satisfactorily by the incorporation of La ions and that the conduction band consists mainly of the 3d and 5d orbitals (coming from Ti) since the contributions of the s and p orbitals are minimal. Electrical conduction takes place mainly in hybrid Ti-O orbitals that the authors call channels. Hashimoto et al.[51] have studied how the conductivity of the material behaved in face of changes in temperature and atmosphere and they have concluded that in a reducing atmosphere

the structure has undergone a significant hysteresis depending on the temperature and, above a concentration of 3% La, the material has a conductivity that is slightly dependent on temperature or partial pressure of oxygen. They also concluded that an oxidizing atmosphere promotes the excess of charges, which causes compensation with the formation of a secondary SrO phase, leading to a decrease in electronic conductivity. Marina *et al.*[52] concluded that SrTiO$_3$ doped with La presents a higher total conductivity when analyzed in a reducing atmosphere. However, Li *et al.*[53] reported that sintering in a reducing atmosphere compensates the A-site deficiencies by charge reorganization, generating oxygen vacancies and increasing the valence of titanium atoms. Therefore, once deficiencies at A-site increase, ionic conductivity also increases (since it is proportional to the concentration of vacancies) and electronic conductivity decreases (because there is less possibility of exchange between the 3+ and 4+ valences of titanium).

Another ion that has shown potential in doping A-site of SrTiO$_3$ structures is yttrium. The band structure of such material was studied by Drozdz *et al.*,[54] the authors show that, when introducing such a dopant, there is a shift in the Fermi level from the bandgap to the conduction band. An increase in the concentration of Y intensifies this shift towards higher energy in the same band and decreases the curvature of the band shape near the base of the conductive band.

Shan and Yi[55] evaluated the electronic conductivity of SrTiO$_3$ structures co-doped with Y and In, as a function of temperature, finding maximum electronic conductivity in the temperature range between 400 and 500 °C. Chen *et al.*[56] observed that these structures exhibit metallic conduction behavior from a temperature of approximately 300 °C, with maximum conductivity also at this temperature, but did not evaluate the behavior at temperatures above 700 °C. They also showed that the concentration of Ti^{3+} ions increases with the dopant increase up to the value of 8%, then remains constant due to the formation of the secondary phase of pyrochlore Y$_2$Ti$_2$O$_7$. Although these studies correlate the electronic conductivity of the material in the face of the effect of temperature and dopant concentration, there is little information about the influence of processing parameters (as in the calcination and sintering steps) on the electrical properties of the material. Gao *et al.*[57] when synthesizing strontium titanate structures doped with yttrium also showed an increase in the concentration of oxygen vacancies that arise to compensate for the decrease in concentration of Ti^{3+}. As this is responsible for electronic conduction, as seen in the state density, it will result in a decrease in electrons in the allowed states of the conduction band. Since compensation is via vacancies, they help to increase ionic conductivity.

Hui and Petric[58] studied the redox behavior of Sr$_{0.88}$Y$_{0.08}$TiO$_{3-}$ and noticed that the variation in electrical conductivity in both the reduction and oxidation processes exhibit parabolic dependence over time. However, the reduction rate is slower than the oxidation rate (Equation 7).

$$O_O^x \leftrightarrow 2e^- + V_{\ddot{O}} + \frac{1}{2}O_{2(g)} \quad (7)$$
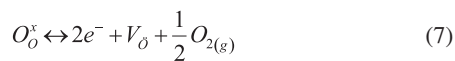
For a material to be a potential candidate as FC anode, the variation in electrical conductivity must be rapid in both oxidation and reduction. The reduction of Sr$_{0.88}$Y$_{0.08}$TiO$_{3-\delta}$ implies the release of oxygen from the network and results in the electrons and vacancies; the reverse process occurs during oxidation. The redox process performance can be described by the following Equation 8.[58]

$$\eta = \frac{\Delta W_t - \Delta W_0}{\Delta W_\infty - \Delta W_0} \quad (8)$$

where ΔW is the weight loss or oxygen variation from stoichiometry

in relation to the theoretical composition, t, 0 and ∞ correspond to arbitrary, initial and final times, respectively. In terms of conductivity, this performance is given by Equation 9: [58]

$$\eta = \frac{\sigma_t - \sigma_0}{\sigma_\infty - \sigma_0} \quad (9)$$

Results showed the conductivity of Sr$_{0.88}$Y$_{0.08}$TiO$_{3-\delta}$ changes quickly at the beginning and reached a plateau, which is a typical behavior of diffusion-controlled processes;[58] it is shown when there was a rapid pressure change on the surface at 800 °C for both processes (oxidation and reduction). Changes in composition must be due to mass transport via diffusion of the gas-solid interface for reduction or vice-versa in oxidation. In the reduction process, the Sr$_{0.88}$Y$_{0.08}$TiO$_{3-\delta}$ nucleus was reduced by the diffusion of oxygen vacancies and at the reduced/oxidized oxide interface whose area decreased with time. The distance from this interface to the surface increased over time, as do the reduction rates or the conductivity decreases over time. For most oxides, diffusion of oxygen at the grain boundary is faster than diffusion in the bulk of grains. As a result, when partial pressure of oxygen is varied, a change in stoichiometry occurs at the grain boundary. They can perform as a reduction path or as a blocking barrier during oxidation.

The performance of Sr$_{0.85}$Y$_{0.10}$Ti$_{0.95}$Ga$_{0.05}$O$_{3-\delta}$ and Sr$_{0.85}$Y$_{0.10}$Ti$_{0.95}$Co$_{0.05}$O$_{3-\delta}$ compounds, using La$_{0.8}$Sr$_{0.2}$Ga$_{0.8}$Mg$_{0.3}$O$_{2.8}$ (LSGM) and YSZ electrolyte, was studied by Hui and Petric.[58] Both compositions resulted in low power densities (maximum value of 58 mW cm^{-2} at 900 °C and partial pressure of O$_2$ 10^{-20} atm) that can be attributed to the high contact resistance between the anode and electrolyte. The ohmic resistance can be reduced by decreasing the thickness of the electrolyte and the electrode with the use of tape manufacturing and laminating techniques, such as tape casting and screen printing of the electrodes.

Hui and Petric[58] also studied the effect of porosity on the conductivity of Sr$_{0.88}$Y$_{0.08}$TiO$_{3-\delta}$ and Sr$_{0.85}$Y$_{0.10}$Ti$_{0.95}$M$_{0.05}$O$_{3-\delta}$ with the addition of 20% (w/w) of carbon. There was a decrease in conductivity in porous samples compared to dense samples. They proposed a mathematical model that agrees with the results obtained experimentally. This model is a relationship between the conductivity of the dense and porous material (σ/σ^0) as a function of the porosity of ceramic materials, and considers that the spherical pores are evenly distributed in the dense materials, as it is shown by Equation 10.

$$\sigma/\sigma^0 = (1 - \varepsilon)/(1 + 0.5\varepsilon) \quad (10)$$

where $\varepsilon = (1 - \rho / \rho_0)$ is the porosity, ρ and ρ_0 are the real and theoretical densities, respectively.

Hui and Petric[58] measured the electrical conductivity of SrTiO$_3$ doped with yttria with different transition metals added as load accepting dopants (M = V, Mn, Fe, Co, Ni, Cu, Zn, Mo, Mg, Zr, Al or Ga) in the temperature range of 600-900 °C in a reducing atmosphere. The substitution of 5% (mol) of Ti by dopants decreases the conductivity of Sr$_{1-1.5x}$Y$_x$TiO$_{3-\delta}$, that is, the degree of conductivity depends on the type of dopant. The catalytic activity of perovskites depends mainly on the ions of the B site, that is, on a metal after its reduction, and its effectiveness in decreasing order can be described as Co > Mn > Ni > Fe > Cr and Sr is the ion from the corresponding A-site that has the best catalytic activity at 800 °C in the partial oxygen pressure range between 10^{-20} and 0.21 atm. Results of the effects of charge acceptor dopants on the conductivity at 800 °C as a function of the partial pressure of oxygen in the compounds Sr$_{0.85}$Y$_{0.10}$Ti$_{0.95}$M$_{0.05}$O$_{3-\delta}$ and Sr$_{0.88}$Y$_{0.08}$Ti$_{0.95}$M$_{0.05}$O$_{3-\delta}$ showed that in

all cases conductivity decreased (except for Co). This is because the conductivity of perovskites depends mainly on the B-O bond strength, the electrons induced by the reduction consequently of the ease of breaking the B-O bond. B, in this case, can be the ions of the transition metals of Co, Mn, Ni, Fe or Cr. Thus, the enthalpy of formation (ΔH^0) of MO_x can be used as an indication of the bond strength of the metal-oxygen in the oxides, in general and ΔH^0 does not depend on the valence of the metal. Conductivity results of $Sr_{0.85}Y_{0.10}Ti_{0.95}M_{0.05}O_{3-\delta}$ and $Sr_{0.88}Y_{0.08}Ti_{0.95}M_{0.05}O_{3-\delta}$ as a function of the bonding strength of oxides V_2O_5, CrO_3, MnO_3, Fe_2O_3, CoO, NiO and CuO showed that the less stable MO bond, easier oxygen forms electronic defects for conduction. Conductivity variation over time at 800 °C was also evaluated, with $Sr_{0.85}Y_{0.10}Ti_{0.95}Co_{0.05}O_{3-\delta}$ having the highest conductivity (17.5 S cm^{-1}) after 24 h of oxidation while in reducing atmospheres ($p_{O_2} = 10^{-19}$ atm) the maximum conductivity obtained was 45 S cm^{-1}. Compounds with the mixed-valence Co^{3+}-Co^{4+} and Mn^{3+}-Mn^{4+} presented high electrical conductivities.

The hypothesis that Sr content decreases the number of oxygen vacancies can be explained by Equation 11,[58] where there is a deficiency limit (x_{lim}) from which perovskite is no longer able to maintain vacancies and new phases will be formed.

$$SrTiO_3 \xrightarrow{Sr\ removal} Sr_{1-x}TiO_{3-x} \xrightarrow{deficiency\ lim\ it} Sr_{1-x\lim}Ti_{1-y}O_{3-x\lim} + y\left(Ti_nO_{2n-1}\right) \quad (11)$$
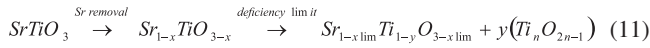
The titanium oxide phases formed when the Sr content was reduced in reducing atmospheres are called Magnelli phases (Ti_nO_{2n-1}, $4 < n < 9$). As strontium titanate has high electrical conductivity in reducing atmospheres, it is interesting to investigate the activity of a multiphase system in which there is high electronic conductivity in both phases (magnelli and strontium titanate). XRD results with different proportions of Sr/Ti showed that the crystalline structures of cubic perovskite and rutile (TiO_2) are present and there is high titanate deficiency (Sr/Ti ≤ 0.9), heated at 1200 °C for 12 h in air. The concentration of the rutile phase was reduced by increasing the Sr/Ti ratio. In titanates with few deficient A sites ($0.01 \leq x \leq 0.05$), the presence of the rutile phase and structures of $Sr_2Ti_6O_{13}$ and $Sr_2Ti_5O_{12}$ were observed. Samples calcined in air with 7% H_2 with reduced deficiency at A sites showed pure structure of cubic perovskite Sr/Ti ≥ 0.98, Magnelli phases being possible impurities. TGA curves showed that the titanate and Magnelli phases were completely oxidized between 600 and 800 °C.[58]

Torabi and Etsell[59] investigated the Yttrium-doped $SrTiO_3$ (YST), deposited in YSZ, as an alternative material to the conventional sulfur and carbon tolerant anode for SOFC. The three samples were infiltrated four times in two heat treatment steps with air (150 °C for 5 min and 350 °C for 15 min). After each infiltration step, the samples were submitted to 3 different types of heat treatments: (a) YST-A was infiltrated four times and treated with air at 900 °C / 6 h, (b) YST-H was infiltrated four times and treated with hydrogen at 900 °C / 6 h and (c) YST-AH was first infiltrated twice, followed by treatment with air at 900 °C/6 h. Then it was infiltrated two more times followed by treatment with hydrogen 900 °C/6 h. Results of EIS with three types of symmetrical YST-YSZ cells (Table 2) showed that the ohmic resistance (R_0) did not vary from one cell to another. However, the non-ohmic resistance showed some differences: an arc at intermediate frequency (100 kHz - 100 Hz) and an arc at low frequency (<100 Hz). The first is attributed to the electron-ion transfer processes at the interface (R_1), and the second is attributed to the unloaded transfer processes (R_2), including surface reactions and gas diffusion in the solid.[60] Table 2 shows that the processes without load transfer were affected by the different heat treatments. The YST-H sample showed the best electrochemical performance (lower R_1 and R_2) compared to the YST-A and YST-A-H samples.

Table 2. Ohmic and non-ohmic polarization of YST cells infiltrated in YSZ with different treatments

Cell	R_0 (Ω cm^2)	R_1 (Ω cm^2)	R_2 (Ω cm^2)
YST-A	0.30	0.28	8.30
YST-A-H	0.29	0.26	2.77
YST-H	0.29	0.20	1.99

Many studies have been presented Y-doped $SrTiO_3$ as a potential alternative material for electrical, electrochemical, and chemical applications due to its mixed (ionic and electronic) conduction and its morphological characteristics.[61]

In the work, Zhao *et al.*,[62] $SrTiO_3$ doped with yttria, deficient at the A (Sr) site, $((Y_{0.08}Sr_{0.92})_{1-x}TiO_{3-\delta})$ was synthesized by the solid-state reaction. The A deficiency limit was lower than 6% (mol) in 5% H_2 in air at 1500 °C. The sinterability of the samples $((Y_{0.08}Sr_{0.92})_{1-x}TiO_{3-\delta})$ decreased with increasing of x deficiency level. The ionic conductivity of $((Y_{0.08}Sr_{0.92})_{1-x}TiO_{3-\delta})$ decreases, while the electronic conductivity reduced with the number of A deficient sites. Chemical analysis of the defects indicated that the introduction of the deficiency at the A-site results not only an increase in oxygen vacancy concentration, but also in decreasing Ti^{3+} concentration.

In the work of Huang *et al.* (2006 (b)),[63] Yttrium-doped strontium titanate ($Y_xSr_{1-x}TiO_3$) was prepared by the solid-state reaction. The maximum electrical conductivity found was with x = 0.08, 71 S cm^{-1} at 800 °C.

In the work of Rosa Silva *et al.*,[64] $SrTiO_3$ was synthesized by solid-state reaction method, calcined, and sintered to obtain undoped (ST), 4% (YST04) and 8% (YST08) of Y-dopant and as a heterojunction with yttria-stabilized zirconia (YST08/YSZ). The effects of calcination atmosphere and dopant concentration on formation of the perovskite and grain size distribution of the material were investigated. It was observed that calcination under Ar/5%H_2 atmosphere increased the dopant maximum concentration in the $SrTiO_3$ cubic crystal structure when compared to inert atmosphere. When the Y solubility limit was exceeded, a pyrochlore phase $Y_2Ti_2O_7$ was formed at the intergranular region due to the deficiency of oxygen vacancies, especially in the presence of inert atmosphere. According to Drozdz *et al.*,[54] the insertion of Y_2O_3 in the crystalline structure of $SrTiO_3$ is conducted as shown by the reaction presented in Equation 12. The donated electrons can occupy empty spaces in the conduction band, create small polarons located in the titanium sites, reduce ions from Ti^{4+} to Ti^{3+} or they can be associated with oxygen vacancies.

$$Y_2O_3 \xrightarrow{SrTiO_3} 2Y_{Sr}^{\bullet} + 2e' + 3O_O^x \quad (12)$$

Thus, in order to replace a Y^{3+} cation at a Sr^{2+} site, there must be enough oxygen vacancies to absorb the three oxygen atoms from Y_2O_3. In the same work, Drozdz *et al.*[54] also showed the effect of the reducing atmosphere on oxygen present in the $SrTiO_3$ structure, as seen in Equation 13. Therefore, when exposing the $SrTiO_3$ structure to a reducing atmosphere, a greater amount of oxygen vacancies appears, and they are necessary for the incorporation of Y^{3+} in the crystalline structure of the perovskite, thus increasing the solubility of the material for this type of doping.

$$O_O^x \xrightarrow{H_2} \frac{1}{2}O_2 + V_{\ddot{O}} + 2e' \quad (13)$$
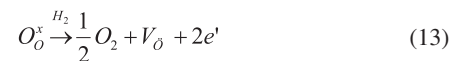
TGA and DTA curves presented a peak of water desorption and two overlapping peaks of $SrCO_3$ phase change and decomposition. Ceramic microstructure was studied by SEM-EDS and the results showed that Y incorporation inhibits the grain growth in sintering step,

reaching a smallest value of grain size in YST08/YSZ heterojunction under Ar/5%H_2 atmosphere.[64]

Curi[65] developed a one-dimensional and isothermal phenomenological mathematical model of ion transport and electronic transport anode bilayer structures MIEC/electrolyte used in SOFC. Performance simulation results showed that yttrium-doped strontium titanate can replace conventional anode because it reached minimal polarization resistance at 670 °C, which is lower than the electronic conduction temperature of the conventional anode Ni/YSZ. Furthermore, the decrease in anode thickness, which reduces the ohmic polarization, also increased the charge transfer rates.

Pyrochlore anodes

Pyrochlores are the only oxides in which simultaneous transformations of order and disorder of cations and anions align the structure. Some crystals have characteristics of allotropy and polymorphism, that is, they exist in more than one crystalline form depending on the conditions of the medium (pressure and temperature). Curi[65] mentioned that the crystalline Ti and Zr structures at room temperature are hexagonal (HC) and at temperatures above 883 °C in the case of Ti and 872 °C, for Zr, they become body-centered cubic (BCC). For Ca it is a face-centered cubic (FCC) at room temperature and BCC at temperatures above 447 °C. This structural change can be explained by the atomic packing factor (APF) and coordination number, which give the metals less energy and stability arrangements. However, HC and FCC crystals have the same APF value (74%) and a coordination number of 12, however, the atomic packing is differentiating them.

Defect pyrochlore oxide powders $ABi_2Ta_5O_{16}$ in pseudo-binary systems $BiTaO_4$-ATa_3O_8 (A=Na, Tl) were prepared by the solid-state method (Ahmed *et al.*, 2019).[66] The structural study showed cubic crystal lattice with *Fd3m* space group to all oxides. The FTIR and Raman bands observed for these compositions are consistent with the Raman spectra expected for defect pyrochlores, $ABBO'_{7-x}$. The morphology of sintering ceramics indicates good densification of the materials. The dielectric constants are in the range of 107-110 with a negative temperature coefficient of permittivity. Dielectric losses of the compound $NaBi_2Ta_5O_{16}$ presented the maximum values versus temperature and frequency, this phenomenon is related to dielectric relaxations. The activation energy and relaxation time τ_0 corresponding these phenomena were found to be 0.16 eV and 0.6×10^{-13} s, respectively. Such dielectric and electrical properties make the compound $NaBi_2Ta_5O_{16}$ attractive in the electrochemical applications.

In pyrochlore oxides ($A_2B_2O_7$), there are different valence combinations in A and B cations, but most of the known pyrochlores, including in the work by Wuensh *et al.*,[67] the phases contain A^{3+} and B^{4+}. Among the physical properties of these materials, the high mobility of oxygen ions is attractive for applications in SOFC.[68] The substitution of species A or B leads to disorder as the substitution reduces the difference between the average radii of the species that occupy these sites. The size difference between the cations can be the driving force for ordering the pyrochlore superstructure. Usually, the replacement of a larger tetravalent cation at the B-site or a smaller trivalent cation at the A-site, or the heating of the phases can lead to some structure disorder, but in the case of pyrochlore oxides, which the strength of the covalent bond is strong, it does not.

In Kaiser *et al.*,[69] $Sr_{0.2}Ba_{0.4}Ti_{0.2}Nb_{0.8}O_3$ was investigated as a material with potential for application as SOFC anode with analysis by EIS and DC conductivity in air under partial oxygen pressure variation at 10 S cm^{-1} ($p_{O2} = 10^{-20}$ atm and 930 °C). EIS measurements show a Warburg-like behavior, indicating that the process is limited

Table 3. SOFC Conductivity for different anode materials as function of temperature and atmosphere

Reference	Anode material	Atmosphere	T (°C)	σ (S cm^{-1})
16	$La_{0.1}Ca_{0.9}TiO_3$	pH_2O/pH_2=0.01	900	50
	$La_{0.1}Ca_{0.9}TiO_3$	Air		0.003
15	$La_{0.4}Ca_{0.6}Cr_{0.2}Ti_{0.8}O_{3-\delta}$	5% H_2/air	1000	50
	$La_{0.05}Ca_{0.95}Cr_{0.2}Ti_{0.8}O_{3-\delta}$	Air		1
17	$Sr_2MgMoO_{6-\delta}$	5% H_2/air	800	42.
	$Sr_2MnMoO_{6-\delta}$			5.4
	$Sr_2MgMoO_{6-\delta}$	H_2		8.6
	$Sr_2MnMoO_{6-\delta}$			8.3
	$Sr_2MgMoO_{6-\delta}$	97% H_2 3%H_2O		8.5
	$Sr_2MnMoO_{6-\delta}$			8.0
	$Sr_2MgMoO_{6-\delta}$	H_2/H_2S		8.5
	$Sr_2MnMoO_{6-\delta}$			7.0
	$Sr_2MgMoO_{6-\delta}$	CH_4		8.5
	$Sr_2MnMoO_{6-\delta}$			11.1
	$Sr_2MgMoO_{6-\delta}$	97% CH_4 3%H_2O		6.6
	$Sr_2MnMoO_{6-\delta}$			10.6
18	$La_{0.60}TiO_{2.90}$	N_2	150	$1.30.10^{-4}$
	$La_{0.58}TiO_{2.87}$			$1.10.10^{-4}$
	$La_{0.57}TiO_{2.86}$			$1.00.10^{-4}$
	$La_{0.55}TiO_{2.83}$			$8.25.10^{-5}$
	$La_{0.54}TiO_{2.81}$			$7.35.10^{-5}$
	$Pr_{0.60}TiO_{2.90}$			$1.65.10^{-5}$
	$Pr_{0.58}TiO_{2.87}$			$1.42.10^{-5}$
	$Pr_{0.57}TiO_{2.86}$			$1.27.10^{-5}$
	$Pr_{0.55}TiO_{2.83}$			$1.10.10^{-5}$
	$Pr_{0.54}TiO_{2.81}$			$9.75.10^{-6}$
20	$La_{0.9}Sr_{0.1}Ga_{0.8}Mn_{0.2}O_3$	H_2-4% air	900	60
21	$La_{0.9}Sr_{0.1}Ga_{0.8}Mn_{0.2}O_3$	Air	700	0.08
			800	0.1
58	$Sr_{0.86}Y_{0.08}TiO_{3-\delta}$	pO_2=10^{-19}atm	800	82
	$Sr_{0.88}Y_{0.08}TiO_{3-\delta}$			64
	$Sr_{0.85}Y_{0.10}Ti_{0.95}Co_{0.05}O_{3-\delta}$			45
58	$La_{0.75}Sr_{0.25}Cr_{0.5}Mn_{0.5}O_3$	pO_2=10^{-19} atm	800	45
22	$La_{0.4}Sr_{0.5}Ti_{0.6}Fe_{0.4}O_{3-\delta}$	Air	900	33.6
		H_2 97% H_2O		1.7
		H_2 10% H_2S		1.6
23	$Sr_{0.97}Ti_{0.6}Fe_{0.4}O_{3-\delta}$		470-870	11.9*
			870-1220	9.35*
	$Sr_{0.90}Ti_{0.6}Fe_{0.4}O_{3-\delta}$		470-890	11.5*
			440-800	8.2*
	$La_{0.4}Sr_{0.5}Ti_{0.6}Fe_{0.4}O_{3-\delta}$		890-1220	12.3*
			840-1060	8.54*
	$Sr_{0.97}Ti_{0.6}Fe_{0.4}O_{3-\delta}$		890-1020	14.2**
			970-1020	13**
25	$La_4Sr_8Ti_{11}Ga_{0.5}Mn_{0.5}O_{37.5}$	Air	900	0.0004
		pO_2=10^{-15}atm		0.5
3	WC		25	$0.52.10^{5*}$
69	$Sr_{0.6}Ba_{0.4}Ti_{0.2}Nb_{0.8}O_3$		930	10*
70	$Gd_2(Ti_{0.3}Mo_{0.7})_2O_7$ $(Gd_{0.9}Ca_{0.1})_2Ti_2O_7$		1000	5.10^{-2**}
71	$Gd_2(Ti_{0.5}Mo_{0.5})_2O_7$		1000	70 / 25

* electronic conductivity, ** ionic conductivity.

Table 4. SOFC power densities for different anode materials as a function of temperature and atmosphere

Reference	Anode	Cathode	Fuel	T (°C)	$P_{máx}$ (mW cm^{-2})
72*	Ni-Cu	$LiNiO_2$	MetOH	600	330
			EtOH		330
73*	Ni-Cu	$LiNiO_2$	Biogas	600	100
				800	700
74*	Ni-Zn	$LiNiO_2$	EtOH	600	353
	Ni-Sn				306
	Ni-Fe				223
75*	$LiNiO_2$	$LiNiO_2$	MetOH	550	512
75*	Ni-Cu-Zn	$LiNiO_2$	MetOH	600	603
				500	431
76*	ZnO/NiO	ZnO/NiO	H_2	520	1257
				500	1107
				480	840
77*	$Li_{0.2}Ni_{0.7}Cu_{0.1}O$/SDC-$Na_2CO_3$	$Li_{0.2}Ni_{0.7}Cu_{0.1}O$/SDC-$Na_2CO_3$	Glycerol	580	215
			Bio-EtOH		148
78 apud 79*	LiCuNiZnO		Bio-EtOH	570	584
80*	C-MO-Ce-O_2		MetOH	560	250
81*	Zn-Ni-Cu	$CuNiO_x$-ZnO	MetOH	580	500
82*	C-(Ni, Cu, Co)O	NiO	MetOH/3% H_2O	550	258
83#	Ru-Ni-GDC	$Sm_{0.5}Sr_{0.5}CoO_3$	Dry CH_4	600	750
			Humidified CH_4		769
			C_2		716
			C_3		648
					769
			H_2	550	511
				525	334
				500	246
84♣	Cu- CeO_2ScSZ $Cu(NO_3)_2Ce(NO_3)_3$ 21.5 % w/w Cu 8.5 % w/w CeO_2	$(Pr_{0.7}Ca0.3)_{0.9}MnO_3$	H_2	800	372
	21.5 % w/w Cu 8.5 % w/w CeO_2			750	234
				700	130
	21.5 % w/w Cu 8.5 % w/w CeO_2		EtOH+H_2O	800	222
				750	139
21▲	$La_{0.9}Sr_{0.1}Ga_{0.8}Mn_{0.2}O_3$	LSC	CH_4	800	88
58●	$Sr_{0.86}Y_{0.08}TiO_{3-δ}$	LSGM	7% H_2	900	58
84♣	20 % w/w Cu 10 % w/w CeO_2 18 % w/w Cu		H_2	800	322
				750	220
				700	122
	12 % w/w CeO_2			800	310
				750	205
				700	122
	15 % w/w Cu 15 % w/w CeO_2	$(Pr_{0.7}Ca0.3)_{0.9}MnO_3$		800	323
				750	201
				700	106
52	CG4	LSM	1.7% CH_4 + 3%H_2O	1000	13.3
			6.7% CH_4+3%H_2O		47
			33% CH_4+3%H_2O		83.9
			4.9% CH_4+ 2%H_2 + 3%H_2O		178.5
25●	$La_4Sr_8Ti_{11}Mn_{0.5}Ga_{0.5}O_{3.5}$	LSM	H_2	950	500
			CH_4		350
17●			H_2	800	968
				700	838
				650	450
	$Sr_2Mg_{0.8}Mn_{0.2}MoO_{6-δ}$		H_2	800	700
			H_2/H_2S		660
	$Sr_2Mg_{0.5}Mn_{0.5}MoO_{6-δ}$		H_2		651
			H_2/H_2S		577
	$Sr_2MnMoO_{6-δ}$		H_2		660
			H_2/H_2S		591
	$Sr_2Mg_{0.9}Cr_{0.1}MoO_{6-δ}$		H_2		790
			H_2/H_2S		610
59●	$Sr_{0.88}Y_{0.08}TiO_3$	LSM	H_2dry	850	95
			CH_4 0.5%H_2S		37

Electrolyte: ●YSZ; *SDC/Na_2CO_3; ▲LSGM; ♣ScSZ; ◻ $BaCe_{0.7}Zr_{0.1}Y_{0.2}O_{3-δ}$ (BCZY)#GDC.

by diffusion. This diffusion limitation may be due to the low ionic conductivity of the oxide or to the layer formed during the sintering of the anode on the electrolyte at temperatures above 1250 °C.

In Kramer and Tuller[70] titanates conducting oxygen ions $(Gd_{1-x}A_x)_2(Ti_{1-y}B_y)_2O_7$ were prepared by the Pechini method.[19] Electron acceptors of sites A (Ca) and B (Al) were incorporated into the $A_2B_2O_7$ structure network. For $Gd_2(Ti_{1-y}Al_y)_2O_7$ the Al $(0 < y < 1)$ solubility was determined using lattice constant measurements by X-ray diffraction, as Al^{3+} is less than Ti^{4+} lattice parameter decreased up to 0.002 Å. For y > 0.01 there was no apparent variation in the lattice constant, thus it was concluded that the limit of solubility of Al^{+3} in $Gd_2(Ti_{1-y}Al_y)_2O_7$ is for y < 0.01. Total electrical conductivity measured in the bulk (σ) of $(Gd_{1-x}Ca_x)_2Ti_2O_7$, x = 0.0025, 0.02, 0.05 and 0.10 as a function of the oxygen partial pressure and temperatures T = 800, 850, 900, 950, 1000, 1050 and 1100 °C showed that for all cases (x and T) for $p_{O_2} \geq 10^{-6}$ σ is independent of the oxygen partial pressure, and for x = 0.005 and 0.10 and T ≤ 900 σ is also independent of the oxygen partial pressure. Ionic conductivity measurements (σ_i) of $(Gd_{1-x}Ca_x)_2Ti_2O_7$ showed that the greater x, and the greater the temperature, the greater the σ_i, in addition, the greater x the smaller the variation in σ_i as a function of temperature. Total electrical conductivity measurements in the $Gd_2(Ti_{0.99}Al_{0.01})_2O_7$ bulk as a function of the oxygen partial pressure showed that for $pO_2 \geq 10^{-10}$ σ is independent of the oxygen partial pressure for all temperatures. At 1000 °C, σ_i $(Gd_{1-x}Ca_x)_2Ti_2O_7$ increased with the increase of x and practically declined with an increase of y in $Gd_2(Ti_{1-y}Al_y)_2O_7$. This result is consistent with the expected since the introduction of accepting impurities Ca^{2+} and Al^{3+} results in the generation of compensating charges for oxygen vacancies. However, the conductivity behavior is slightly different from the linear dependence predicted by the models proposed in the article.

Table 3 summarizes main studies in the literature on electrical conductivity (electronic + ionic) of anodic materials with respective operation temperature and measurement atmosphere (oxidizing or reducing atmosphere). Although there are other anodic materials, such as fluorite and carbide anodes, those were not the focus of this work.

In Table 4, there is a summary of the SOFC power densities for different anode materials, operating temperature, and fuel. Comparing the same anodic material, using the same fuel and the same cathode, in all cases the SOFCs showed higher power density at higher temperatures. Increasing the CH_4 concentration increases the SOFC power density, applying CG4 as an anode and LSM as the cathode. In studies that analyzed the influence of the fuel, SOFCs with anodes powered by pure H_2 tended to present a higher power density than those powered by hydrogen mixture, H_2/H_2S or other fuels (CH_4, C2, C3, and EtOH). The infiltration of the WC anode increased the power density compared to the conventional WC anode for the same operating temperature.

CONCLUSIONS

In this work, the authors had the approach of reviewing a large number of published works about materials applied to SOFC anodes. First, we concluded that the currently used material composed by a *cermet* of Ni/YSZ is not applicable to the new requirements such as the feed with other types of fuels and temperature operation. Subsequently, different types of promissory candidates were discussed, concluding that perovskite compounds are structures with great potential for this kind of application once they are stable under a reducing atmosphere and can be easily synthesized. The major advantage of perovskite anodes is the possibility of changing the physical-chemical characteristics (such as electronic/ionic conductivity and thermal expansion) through doping processes. Many different types of cations can be used as dopants in the A and B sites of the compounds, generating different semiconductors with distinct redox properties and electrocatalytic activity. Among those candidates, the material with mixed, ionic and electronic conductivity consisted by yttrium doped-$SrTiO_3$ stands out as a promising candidate as it can be operated with hydrocarbons fuels (once it does not catalyze the breakage of carbon bonds) at lower temperatures when compared to the operation with Ni/YSZ anodes. These structures showed a satisfactory performance regarding its conductivity, mainly when doped with 8% of the Y cation. However, at this concentration, the solubility limit of the dopant is reached and a secondary phase of pyrochlore is formed, this phase presents an electric insulating character. Hence, it was concluded that the presence of a reducing agent in the calcination atmosphere decreases this insulating phase concentration, improving conductivity. Although the research about adequate materials for SOFC anode is advanced and satisfactory, there are still many challenges in the future such as a significant reduction in the operation temperature ($\sim$300 – 600 °C), a deeper understanding on the reaction mechanisms of generation and degradation, and constant optimization of electrodes morphology to improve efficiency.

ACKNOWLEDGEMENTS

REFERENCES

1. Fiuza, R. P.; Silva, M. A.; Pontes, L. A. M.; Teixeira, L. S. G.; Boaventura, J. S.; *Quim. Nova* **2012**, *35*, 1635.

2. Amado, R. S.; Malta, L. F. B.;Garrido, F. M. S.; Medeiros, M. E.; *Quim. Nova* **2007**, *30*, 189.

3. Torabi, A., Etsell, T. H.; *J. Power Sources* **2012**, *212*, 47.

4. Curi, M. O.; Silva, E. R.; Secchi, A. R.; Furtado, J. G. de M.; Ferraz, H. C.; *XXI Congresso Brasileiro de Engenharia Química*, Fortaleza, Brasil, 2016.

5. Tarôco, H. A.; Santos, J. A. F.; Domingues, R. Z.; Matencio, T. In *Ceramic Materials for Solid Oxide Fuel Cells*; Sikalidis, C., ed.; InTech: London, 2011, cap. 19.

6. Matsuzaki, Y.; Yasuda, I.; *Solid State Ionics* **2000**, *132*, 261.

7. Lussier, A.;Sofie, S. W.; Dvorak, J.; Idzerda, Y. U.; *Int. J. Hydrogen Energy* **2008**, *33*, 3945.

8. Flores, J.A.; Rodríguez, L. A.; *Revista Mexicana de Física* **2013**, *59*, 66.

9. Sun, C.; Stimming, U.; *J. Power Sources* **2007**, *171*, 247.

10. Curi, M. O.; *Dissertação de Mestrado*, Universidade Federal do Rio de Janeiro, Brasil, 2011.

11. Magalhães, R. S.; Junior, W. D. M.; Souza, A. E.; Teixeira, S. R.; Li, S. M.; Longo, E.; *Quim. Nova* **2017**, *40*, 166.

12. Meulenberg, W. A.; Ivanova, M. A.; Serra, J. M.; Roitsch, S. In *Advanced Membrane Science and Technology for Sustainable Energy and Environmental Applications*; Basile A., Nunes, S. P., eds.; Woodhead Publishing Limited: Cambridge, 2011, cap. 17.

13. Raphael, E.; Silva, M. N.;Szostak, R.; Schiavon, M. A.; Nogueira, A. N.; *Quim. Nova* **2018**, *41*, 61.

14. Yang, L.; Dacek, S. T.; Ceder, G.; *Phys. Rev. B* **2014**, *90*, 54102.

15. Vashook, V.; Vasylechko, L.; Knapp, M.; *J. Alloys Compd.* **2002**, *354*, 13.

16. Vashook, V.; Vasylechko, L.; Ullmann, L.H.; Guth, U.; *Solid State Ionics* **2003**, *158*, 263.

17. Huang, H.Y.; Dass, R. I.; Xing, X. L.; Goodenough, J. B.; *Science* **2006**, *312*, 254.

18. Lepe, F. J.; Fernandez-Uurban, J.; F.; Mestres, L.;Martínez-Sarrión, M. L.; *J. Power Sources* **2005**, *151*, 74.

19. Pechini, M. P.; *US pat.* 3,330, *697*, **1967**.

20. Pudmich, G.; Boukamp, B. A.; Gonzalez, M. C.; *Solid State Ionics* **2000**, *135*, 433.

21. Chen, F.; Liu, M..; *J. Solid State Electrochem*. **1998**, *3*, 7.

22. Zha, S.; Tsang, P.; Cheng, Z. J.; Liu, M.; *J. Solid State Chem.* **2005**, *178*, 1844.

23. Fagg, D. P.;Kharton, V. V.; Kovalevsky, A.V.; Naumovich, E. N.; Frade, J. R.; *J. Eur. Ceram. Soc.* **2001**, *21*, 1831.

24. Kharton, V. V.; Kovalevsky, A. V.; Viskup, A. P.; Figueiredo, F. M.; Frade, J. R.; Yaremchenko, A. A.; Naumovich, E. N.; *Solid State Ionics* **2000**, *128*, 117.

25. Ruiz-Morales, J. C..; Canales-Vázquez, J.; Savaniu, C.; Marrero-López, D.; *Nature* **2006**, *439*, 568.

26. Vernoux, P.; Guillodo, M.; Fouletier, J., Hammou, A.; *Solid State Ionics*. **2000**, *135*, 425.

27. Vernoux, P.; Djurado, E.; Guillodo, M.; *J. Am. Ceram. Soc.* **2001**, *84*, 2289.

28. Sfeir, J.; *J. Power Sources* **2003**, *118*, 276.

29. Neagu, D.; Irvine, J. D. S. In *Comprehensive Inorganic Chemistry II*; Reedijk, J., Poeppelmeier, K., eds.; Elsevier: Amsterdam, 2013, cap. 4.15.

30. Ma, Q.; Iwanschitz, B.; Dashjav, E.; Baumann, S.; Sebold, D.; Raj, I. A.; Mai, A.; Tietz, F.; *J. Power Sources* **2015**, *279*, 678.

31. Chen, C.; Zhang, T.; Donelson, R.; Tan, T. T.; Li, S.; *J. Alloys Compd.* **2015**, *629*, 49.

32. Marques, A. C.; *Tese de Doutorado*, Faculdade de Ciências da Universidade de Lisboa, Portugal, 2009.

33. Muhamad, N. F.; Osman, R. A. M.; Idris, M. S.; Yasin, M. N. M.; *EPJ Web of Conferences* **2017**, *162*, 1052.

34. Suwanwong, S.; Eknapakul, T.; Rattanachai, Y.;Masingboon, C.; Rattanasuporn, S.; Pattanakun, R.; Nakajima, H.; King, P.; Hodak, S. K.; Meevasana, W.; *Appl. Surf. Sci.* **2015**, *355*, 210.

35. Mohamed, E. A.; Moustafa, M. G.; Kashif, I.; *J. Non-Cryst. Solids* **2018**, *482*, 223.

36. Shackelford, J. F. In *Ciência dos Materiais*; Sousa, A., Pace, M., eds.; Pearson Publishing: London, 2008.

37. Kharton, V. V.; Kovalevsky, A. V.; Viskup, A. P.; Jurado, J. R.; Figueiredo, F. M.; Naumovich, E. N.; Frade, J. R.; *J. Solid State Chem.* **2001**, *156*, 437.

38. Flores, J. J. A.;Rodríguez, M. L. A.; Espinosa, G. A.; Vera, J. V. A.; *Int. J. Hydrogen Energ.* **2018**, *44*, 12529.

39. Steinsvik, S.; Bugge, R.; Gjonnes, J.; Norby, J. T. T.; J. *Phys. Chem. Solids* **1997**, *6*, 969.

40. Kubacki, J.; Kajewski, D.; Goraus, J.; Szot, K.; Koehl, A.; Lenser, C.; Dittmann, R.; Szade, J.; *J. Chem. Phys.* **2018**, *148*, 154702.

41. Baker, J. N.; Bowes, P. C.; Long, D. M.; Moballegh, A.; Harris, J .S.; Dickey, E. C.; Irving, D. L.; *Appl. Phys. Lett.* **2017**, *110*, 122903.

42. Li, R.; Liu, F.; Zhang, C.; Liu, J.; Zhou, J.; Xu, L.; *Ceram. Int.* **2019**, *45*, 21684.

43. Morin, F. J.; Oliver, J. R.; *Phys. Rev. B* **1973**, *8*, 5847.

44. Zhao, Z.; Gonçalves, R. V.; Barman, S. K.; Willard, E. J.; Byle, E.; Perry, R.; Wu, Z.; Huda, M. N.; Moulé, A. J.; Osterloh, F. E.; *Energy Environ. Sci.* **2019**, *12*, 1385.

45. Bowes, P. C.; Baker, J. N.; Irving, D. L.; *J. Am. Ceram. Soc.* **2019**, *00*, 1.

46. Smith, H. B.; Holler, W. C.; Gross, M. D.; *Solid State Ionics* **2011**, *192*, 383.

47. Zhang, C.; Wang, C. L.; Li, J. C.; Yang, K.; Zhang, Y. F.; Wu, Q. Z.; *Mater. Chem. Phys.* **2008**, *107*, 215.

48. Blennow, P.; Hagen, A.; Hansen, K. K., Wallenberg, L. R.; Mogensen,

M.; *Solid State Ionics* **2008**, *179*, 2047.

49. Ozdogan, K.; Kahaly, M. U.; Kumar, S. R. S.; Alshareef, H. N.; Schwingenschlögl, J.; *J. Appl. Phys.* **2012**, *111*, 054313.

50. Biswas, A.. Li, N.; Jung, M. H.; Lee, Y. W.; Kim, J. S.; Jeong, Y. H.; *J. Appl. Phys.* **2013**, *113*, 183711.

51. Hashimoto, S.; Kammer, K.; Larsen, P. H.; Finn, L.; Poulsen, F. W.; Mogensen, M.; *Solid State Ionics* **2005**, *176*, 1013.

52. Marina, O. A.; Canfield, N. L.; Stevenson, J. W.; *Solid State Ionics* **2002**, *149*, 21.

53. Li, X.; Zhao, H.; Zhou, X; Xu, N.; Xie, Z.; Chen, N.; *Int. J. Hydrogen Energy* **2010**, *35*, 7913.

54. Drozdz, E.;Lacz, A., Kolezynzky, A.;Mikula, A.; Mars, K.; *Solid State Ionics* **2017**, *302*, 173.

55. Shan, K.; Yi, Z.; *Scr. Mater*. **2015**, *107*, 119.

56. Chen, C.; Zhang, T.; Donelson, R.; Tan, T. T.; Li, S.; *J. Alloys Compd.* **2015**, *629*, 49.

57. Gao, F.; Zhao, H.; Li, X.; Cheng, Y.; Zhou, X.; Cui, F.; *J. Power Sources* **2008**, *185*, 26.

58. Hui, S.; Petric, A.; *Mater. Res. Bull.* **2002**, *37*, 1215.

59. Torabi, A.; Etsell, T. H.; *J. Power Sources* **2013**, 225, 51.

60. Tarôco, H. A.;Andrade, S. T. P.;Brant, M. C.; Domingues, R. Z.; Matencio, T.; *Quim. Nova* **2009**, *32*, 1297.

61. Rosa Silva, E.; Nicolini, J. V.; Yamauchi Jr., L.; Machado, T. M.;Curi, M.; Furtado, J. G.; Secchi, A. R.; Ferraz; H. C.; *Ceram. Int.* **2020**, *46*, 3592.

62. Zhao, H.; Gao, F.; Li, X.; Zhang, C.; Zhao, Y.; *Solid State Ionics* **2009**, *180*, 193.

63. Huang, X.; Halei, Z.; Shen, W.; Qiu, W.; Wiu, W.; *J. Phys. Chem. Solids* **2006**, *67*, 2609.

64. Rosa Silva, E.; Curi,M.; Furtado, J. G.; Secchi, A. R.; Ferraz; H. C.; *Ceram. Int.* **2019**, *45*, 9761.

65. Curi, M. O.; *Tese de Doutorado*, Universidade Federal do Rio de Janeiro, Brasil, 2015.

66. Ahmed, O. A. S.; Bourja, L.; Chagraoui, A.; Tairi, A.; Moussaoui, A.; Oulahyane, H. A.; Manoun, H.; Villain, S.; *Heliyon* **2019**, *5*, 1891.

67. Wuensh, B. J.; Eberman, K. W.; *Journal of Sedimentary Environments* **2000**, *52*, 19.

68. Pirzada, M.; Grimes, R. W.;Minervini, L.;Maguire, J. F.; Siackafus, K. E.; *Solid State Ionics* **2001**, *140*, 201.

69. Kaiser, A.; Bradley, J. L.; Slater, P. R.; Irvine, J. T. S.; *Solid State Ionics* **2000**, *135*, 519.

70. Kramer, S.A.; Tuller, H. L.; *Solid State Ionics* **1995**, *82*, 15.

71. Porat, O.; Heremans, C.; Tuller, H.L.; *Solid State Ionics* **1997**, *80*, 2278.

72. Zhu, B.; *J. Power Sources* **2001**, *93*, 82.

73. Zhu, B.; Bai, X. Y.; Chen, G. X.; Yi, W. M.; Bursell, M.; *Int. J. Energy Res.* **2002**, *26*, 57.

74. Huang, J.; Xie, F.; Wang, C.; Mao, Z.; *Int. J. Hydrogen Energy* **2012**, *37*, 877.

75. Gao, Z.; Raza, R.; Zhu, B.; Mao, Z.; Wang, C.; Liu, Z.; *Int. J. Hydrogen Energy* **2011**, *36*, 3984.

76. Raza, R.; Liu, Q.; Nisar, J.; *Electrochem. Commun.* **2011**, *13*, 917.

77. Qin, H.; Zhu, Z.; Liu, Q.; *Energy Environ. Sci.* **2011**, *4*, 1273.

78. Imaran, S. K.; Raza, R.; Abbas, G.; Zhu, B.; *J. Fuel Cell Sci. Technol.* **2011**, *8*, 1.

79. Fan, L.; Wang, C.; Chen, M.; Zhu, B.; *J. Power Sources* **2013**, *234*, 154.

80. Feng, B.; Wang, C. Y.; Zhu, B.; *J. Electrochem. Soc.* **2006**, *9*, 80.

81. Mat, M. D.; Liu, X., Zhu, Z.; Zhu, B.; *Int. J. Hydrogen Energy* **2006**, *32*, 796.

82. Xu, S.; Niu, X.; Chen, M.; Wang. C.; *J. Power Sources* **2007**, *165*, 82.

83. Hibino, T.; Hashimoto, A.; Yano, M.; Suzuki, M.; Sano, M.; *Electrochim. Acta* **2003**, *48*, 2531.

84. Ye, X. F.; Huan, B.; Wang, S. R.; Wang, Z. R.; Xiong, L., Wen, T. L.; *J. Power Sources* **2007**, *164*, 203.